A Simple Collisional-Radiative Model Applicable to Argon Arcjet

IEPC-2013-190

Presented at the 33rd International Electric Propulsion Conference,
The George Washington University • Washington, D.C. • USA
October 6 – 10, 2013

Su-Rong Sun[1] and Hai-Xing Wang[2]
School of Astronautics, Beijing University of Aeronautics and Astronautics, Beijing, 100191, China

Abstract: A simple collisional-radiative model is applied to argon arcjet in order to investigate the dominant chemical reactions in the plasma flow. The kinetic processes taken into account in this paper include spontaneous emission, electron impact ionization, three body recombination, excitation and deexcitation between different excited levels, electron ion radiative recombination. The modeling results are the populations of the various excited levels as a function of distance, and the relative contributions of different populating and depopulating processes for excited levels. The main production and loss processes determine the excited argon atoms and ions densities are also presented inside the constrictor and expansion portion of the nozzle.

Nomenclature

ρ_i	=	mass density of species *i*
$\vec{J}_i$	=	diffusion mass flux density vector of species *i*
$\vec{u}$	=	mass-averaged velocity of species *i*
$\dot{\rho}_i^k$	=	unidirectional chemical rate of change of ρ_i
$f(\varepsilon)$	=	electron energy distribution function
ε	=	electron energy
$\sigma(\varepsilon)$	=	inelastic collision cross section
n_i	=	number densities of species *i*
Q	=	chemical reaction rate coefficient
A	=	Einstein coefficient

I. Introduction

Arcjet thrusters have already been successfully used for satellite north-south station-keeping for several decades [1, 2]. In order to improve arcjet efficiency and extend the operating range, the main physical and chemical kinetics mechanisms inside arcjet should be examined in detail. Due to the small size of the constrictor and nozzle length, the plasma flow inside arcjet thruster is characterized by the extremely high temperature and velocity gradient. Over the past several decades, although much effort has been devoted to the development of comprehensive physical models to describe the plasma flow inside arcjet thruster, questions remain concerning the plasma reaction kinetics features of the high velocity plasma flow within arcjet thrusters. In this paper, a zero-dimensional collisional-radiative model is proposed to study chemical reactions in plasmas system encountered in arcjet thruster. The collisional-radiative model allows the identification of the main processes responsible of the excited atom concentrations.

[1] Graduate Student, sunsurong@sa.buaa.edu.cn.
[2] Professor, whx@buaa.edu.cn.

The classical approach to collisional-radiative models (CR Model) is the quasi-stationary state approximation introduced by Bates et al. [3]. This model is based on the assumption that the relaxation times of excited levels are orders of magnitude shorter than ionization / recombination ones. In these conditions the level distributions are stationary with respect to electron and ground state population densities, simplifying the solution of the problem. Later, the time-dependent solution of kinetic equations is developed for situations characterized by very short macroscopic relaxation times. Numerous models [4-7] have been presented for various atoms calculating time-dependent solutions of collisional-radiative models. The interest of a time-dependent approach is the possibility to follow the temporal relaxation of atomic level populations and then to study the validity of the quasi-steady-state hypothesis. Thus the collisional-radiative model allows for the calculation of global rate coefficient: the rate coefficients of ionization, recombination or dissociation.

In the present paper, we propose to focus our attention on the kinetics mechanisms inside arcjet. So the steady state solution of excited states kinetics has been elaborated without calculating directly the time evolution of the species only due to the various chemical processes involved. The plasma flow parameters inside an arcjet (electron density, electron temperature, pressure and heavy particle temperature distributions) are obtained from nonequilibrium modeling of the plasma flow inside arcjet thruster [8]. The results of the kinetic processes have been presented along the nozzle axis and radial direction.

II. Characteristic Time Scales of Plasma Flow Inisde Arcjet

Since the plasma flow through the constrictor and nozzle with a high velocity, the fluid dynamical time scales are comparable to the chemical reaction time scales [9, 10]. Here we compare the typical chemical reaction time scales with those for convection and diffusion to analyze the adaptability of steady state solution of CR model for this case. The time scale for species density changes due to fluid expansion or contraction is

$$t_e = \frac{1}{\left|\vec{\nabla} \cdot \vec{u}\right|} \tag{1}$$

The convective time scale is defined as

$$t_c = \frac{\rho_i}{\left|\left(\vec{\nabla}\rho_i\right) \cdot \vec{u}\right|} \tag{2}$$

The time scale for diffusion of species is defined as

$$t_d = \frac{\rho_i}{\left|\vec{\nabla} \cdot \vec{J}_i\right|} \tag{3}$$

The local chemical time scale for the reaction *k* is

$$t_k = \frac{\rho_i}{\left|\dot{\rho}_i^k\right|} \tag{4}$$

where ρ_i is the mass density of species *i*, $\vec{u}$ is the mass-averaged velocity of species *i*, $\vec{J}_i$ is the diffusion mass flux density vector of species *i*, $\dot{\rho}_i^k$ is the unidirectional chemical rate of change of ρ_i .

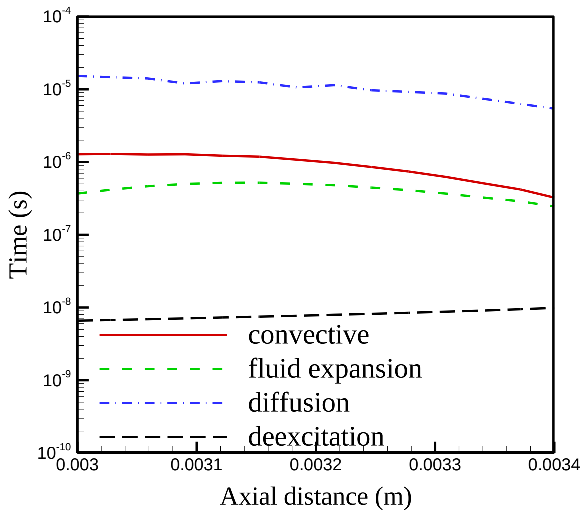

Figure 1. Time scales for deexcitation along the constrictor axis

Figure 1 shows the time scales of various processes in plasmas along the constrictor axis. The time scales of transport processes are seen to be larger than the time scales of de-excitation process along the axis, where the de-excitation reaction is electron impact metastable state de-excitation. Therefore, neglecting the effects of convective and diffusion transport on the species distribution and chemical reaction process in CR model is reasonable for this case. Although the discrepancies may exist between calculated and practical population number densities, the chemical reaction mechanism inside arcjet can be clearly clarified.

III. Collisional Radiative Model

The system studied in this work is a plasma formed by atomic argon including ground state and excited states (Ar), argon atomic ions (Ar^+), argon molecular ions (Ar_2^+), argon excimer molecules (Ar_2^*) and electrons. We assume that the plasma is electric neutrality. The plasma has been considered optically thin (photon absorption and photoionization have been neglected). The distributions of energies of particles are assumed Maxwellian.

A. Electron Induced Processes

The electron induced processes include electron impact excitation and deexcitation processes, electron impact ionization and three body recombination processes. Reaction rate coefficients for electron induced processes are calculated from electron energy distribution functions (EEDF) using the equation:

$$C_{ij} = \int_{E_{\min}}^{\infty} f(\varepsilon)\sigma(\varepsilon)v(\varepsilon)d\varepsilon \tag{5}$$

where $f(\varepsilon)$ represents the EEDF, $\sigma(\varepsilon)$ the cross section of the transition between atomic levels *i* and *j*, $v(\varepsilon)$ the velocity of the electron of kinetic energy ε and E_{min} the threshold energy of the process. The experiment measurement of excitation cross section has been used instead of those from the empirical formula [11, 12]. The rate coefficients of inverse processes are calculated by the principle of detailed balancing. The dominant excitation processes are taken from the literature [13].

B. Radiative Recombination

Only the transitions straightforward to the ground state and the $3p^5 4s$ levels are considered in this study. The radiative recombination process is neglected for high lying excited states since the radiative recombination cross section depends on n_i^{*-3} where n_i^* is the effective quantum number [14]. The plasma is assumed to be optically thin to the continuum radiation due to recombination processes. The recombination rate coefficient to the ground state is derived from the literature [15]. The radiative recombination cross section adopted for other processes is given in the reference [11].

C. Spontaneous Emission

The rate of radiative decay is given by the Einstein transition probability, multiplied by an escape factor, describing the effect of ‘radiation trapping’. The transition probabilities were adopted from more recent results of Wiese et al. [16] as basic data. We assume the escape factors to be equal to 1 (*i.e.*, 100% escape of radiation, no radiation trapping).

D. Inelastic Atom-Atom Collisions

For the atom impact excitation processes, the models retained by reference [13] are used. The reaction rate coefficients of inverse processes are calculated by the principle of detailed balancing. For ground state atom ionization process, the ionization cross section measured by Haugsjaa and Amme [17] is used. For atom impact three body recombination process, the reaction rate coefficient is taken from the literature [18].

E. Other Processes

Finally, some additional processes were included in the model. These processes include penning ionization of argon 1s states, the three-body collisional association to form excimers and molecular ions, the electron-impact dissociation of excimers and molecular ions, the atom-collision dissociation of excimers and molecular ions, the electron collisional recombination for molecular ions. The reaction rate coefficients for excimers and molecular ions are taken from the reference [14, 19, 20].

F. Master Equation

Taking into account the different elementary processes mentioned above, the rate equations for the production of an excited atom on the level *i* in steady state can be written as

$$\begin{aligned} & n_e \sum_{y \neq x} n_y Q^{e}_{y \to x} + n_g \sum_{y \neq x} n_y Q^{at}_{y \to x} + \sum_{y \neq x} A_{y \to x} n_y + n_e^2 n_{Ar^+} Q^{rec} + n_e n_{Ar_2^+} Q^{rec} + n_e n_{Ar_2^*} Q^{e-dis} + n_g n_{Ar_2^*} Q^{at-dis} = \\ & n_e n_x \sum_{y \neq x} Q^{e}_{x \to y} + n_g n_x \sum_{y \neq x} Q^{at}_{x \to y} + A_{x \to gs} n_x + \sum_{y \neq x} A_{x \to y} n_x + n_e n_x Q^{ion} + 2 n_x^2 Q^{penni}_{x,x} + \\ & n_x \sum_{y \neq x} n_y Q^{penni}_{x,y} + n_{Ar_2^*} n_x Q^{penni}_{x, Ar_2^*} + n_g^2 n_x Q^{3-body} \end{aligned} \tag{6}$$

The rate balance equation of Ar_2^*:

$$\begin{aligned} & n_g^2 \sum_{x} n_x Q^{3-body} = n_e n_{Ar_2^*} \sum_{x} Q^{e-dis}_{Ar_2^* \to x} + n_g n_{Ar_2^*} \sum_{x} Q^{at-dis}_{Ar_2^* \to x} + A_{Ar_2^*} n_{Ar_2^*} \\ & + n_e n_{Ar_2^*} Q^{ion} + 2 n^2_{Ar_2^*} Q^{penni}_{Ar_2^*, Ar_2^*} + n_{Ar_2^*} \sum_{x} n_x Q^{penni}_{x, Ar_2^*} \end{aligned} \tag{7}$$

The rate balance equation of Ar_2^+:

$$\begin{aligned} & n_g^2 n_{Ar^+} Q^{3-body} + n_e n_{Ar_2^*} Q^{ion} + n^2_{Ar_2^*} Q^{penni}_{Ar_2^*, Ar_2^*} + n_{Ar_2^*} \sum_{x} n_x Q^{penni}_{x, Ar_2^*} + n_x^2 Q^{ion}_{meta-meta} = \\ & n_e n_{Ar_2^+} Q^{e-dis} + n_g n_{Ar_2^+} Q^{at-dis} + n_e n_{Ar_2^+} \left(Q^{rec}_{Ar_2^+ \to gs} + \sum_{x} Q^{rec}_{Ar_2^+ \to x} \right) \end{aligned} \tag{8}$$

The rate balance equation of Ar^{2+}:

$$n_e n_{Ar^+} Q^{ion} = n_e^2 n_{Ar^{2+}} Q^{rec} \tag{9}$$

The electrical neutrality of the plasma:

$$n_{Ar^+} + n_{Ar_2^+} + 2 n_{Ar^{2+}} = n_e \tag{10}$$

The state equation:

$$\begin{aligned} & p = n_e k_B T_e + n_g k_B T_h + \sum_{x} n_x k_B T_h + \\ & n_{Ar_2^*} k_B T_h + n_{Ar_2^+} k_B T_h + n_{Ar^+} k_B T_h + n_{Ar^{2+}} k_B T_h \end{aligned} \tag{11}$$

Here n_e refers to the electron density, n_g is the gas density and the other subscripts of *n* (*x*, *y*, Ar^+, Ar_2^+, Ar_2^*) denote the excited or ionized particles. *Q* is the reaction rate coefficient and *A* is the Einstein coefficient. In each set of calculations, T_e, T_h and *p* are constant.

IV. Computational Results

G. Chemical kinetic processes inside constrictor

Fig. 2 shows the axial profiles of argon atom ground state, argon atom excited states, excimers, argon ions and molecular ions number densities along the axis of the constrictor. It can be seen from this figure that the number density of Ar^+ ions is lower than that of ground state of argon atom while higher than the number densities of other particles, and some of Ar^+ ions are ionized to produce Ar^{2+}. The number densities of argon excimers and molecular ions can be neglected in the center of constrictor. Figure 3 shows different ionization and recombination mechanisms along the constrictor axis. It is shown that electron impact high lying excited states ionization is dominant ionization process, while electron impact ground state ionization process is weaker than high lying excited states ionization. Atom impact ionization reactions play a minor role in total ionization mechanisms. The dominant recombination process is electron impact three body recombination to high lying excited states. The radiative recombination and atom impact three body recombination processes have a small influence on total recombination mechanisms.

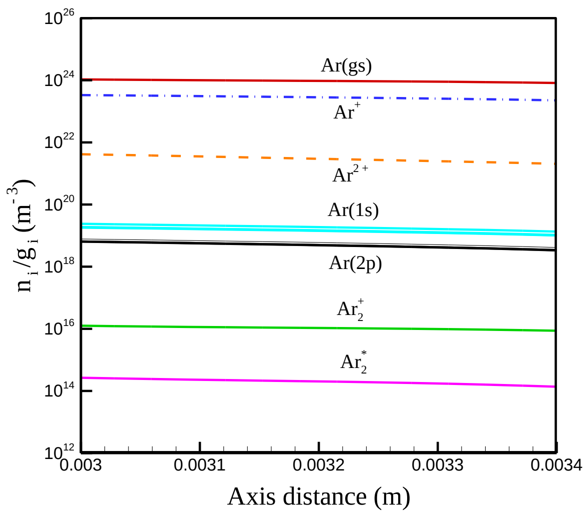

Figure 2. Axial profiles of plasma composition along the constrictor axis.

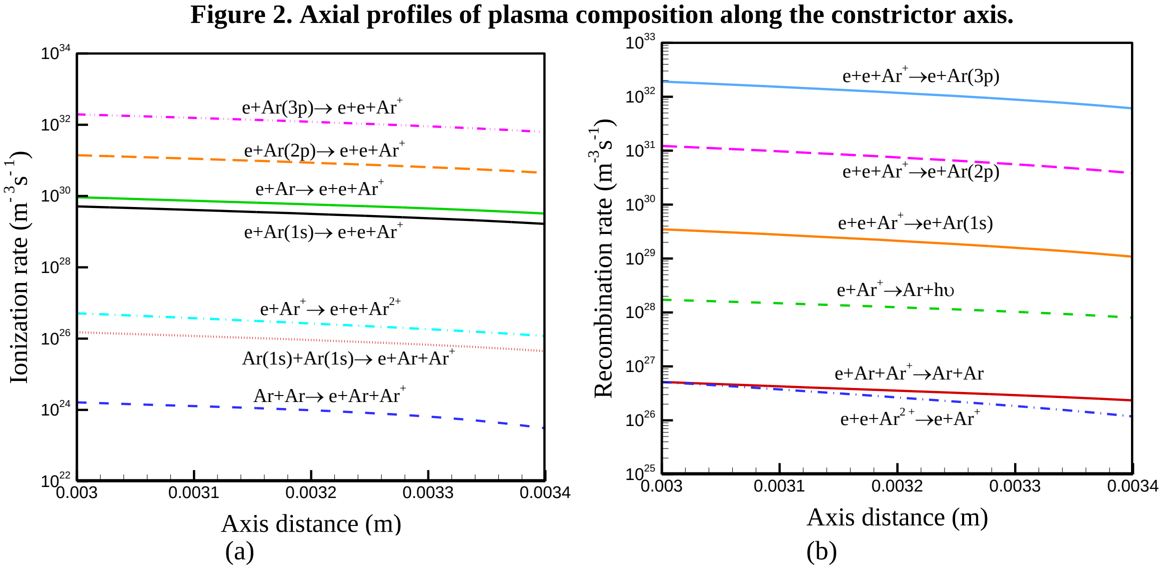

Figure 3. Axial profiles of ionization (a) and recombination (b) mechanisms along the constrictor axis.

Figure 4 shows the axial profile of plasma composition along the inner wall of constrictor. It is found that different from the composition along the axis, the argon molecular ions and excimers play an important role. It should be noted that the number densities of Ar^+ ions are lower than that of molecular ions. With the increase of temperature along the wall, the number densities of argon excited states increase. Figure 4 also shows axial profiles of production and loss rate of argon excimers along the constrictor wall. It can be seen that argon excimers are created by argon atom three-body collisional association process. Because of the high number densities of argon atom, the atom-collision dissociation of excimers is dominating loss channel. Radiation of excimers also contributes to the loss mechanism. Penning ionization of argon excimers and electron-impact ionization reaction have a small influence on the loss mechanisms. Figure 5 further shows the axial profile of production and loss rate of molecular ions along the wall. It is seen that the Ar_2^+ ions are mainly created by atomic ions to molecular ions conversion, whereas metastable-metastable associative ionization and penning ionization of argon excimers seem to play only a minor role at the wall. Loss of these Ar_2^+ ions is caused primarily by the dissociative recombination to the ground state, but electron impact dissociation in the plasma plays also a significant role, especially at the downstream of wall. Atom impact dissociation process can be neglected.

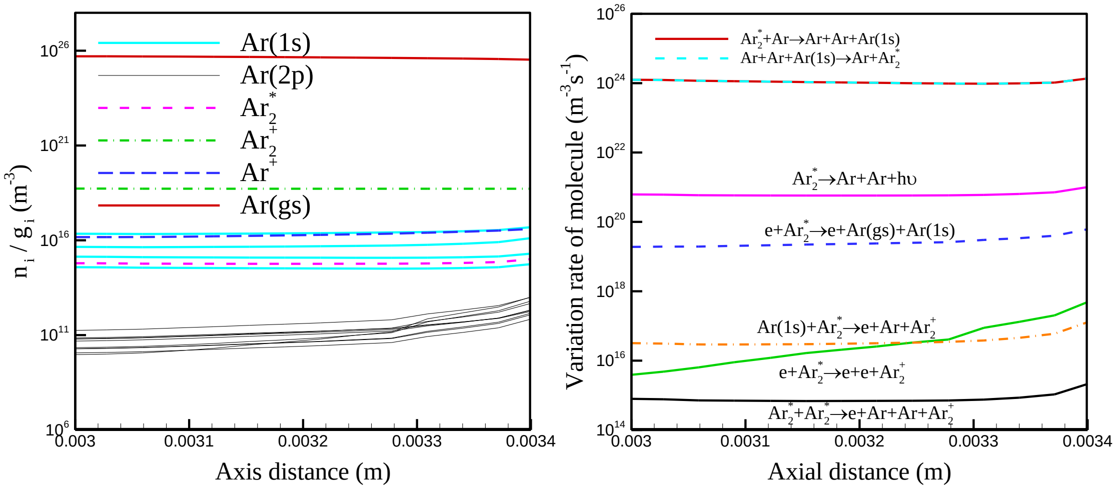

(a) (b)

Figure 4. Axial profiles of plasma composition (a) and production and loss rate of argon excimers (b) along the constrictor wall.

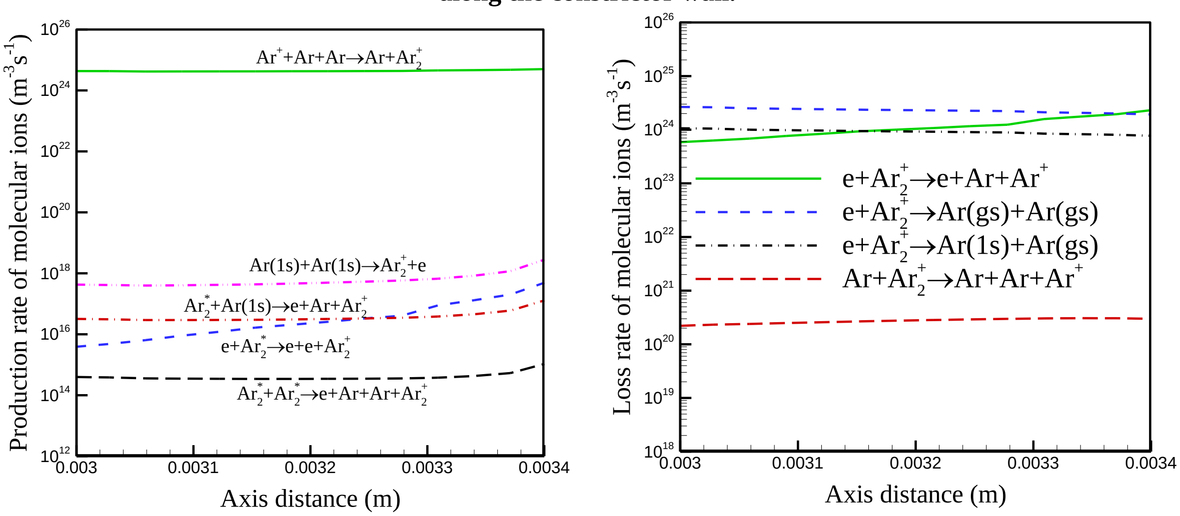

(a) (b)

Figure 5. Axial profiles of production (a) and loss (b) of molecular ions along the constrictor wall.

Figure 6 shows radial profiles of plasma composition along the constrictor outlet. The number densities of atomic ions gradually decrease from the center to wall. The number densities of molecular ions firstly increase, then decrease to the wall. Molecular ions become more important at the constrictor wall. The excited states have the same trend because of the decreased temperature. Figure 7 shows radial profiles of production and loss processes of metastable state ($1s_5$) along the constrictor outlet. The main production processes of $1s_5$ state are electron impact 2p levels deexcitation and electron impact resonance state deexcitation at the beginning of constrictor axis, then atom collision dissociation of excimers and atom impact 2p levels deexcitation become more and more important at the wall. Electron collisional recombination for molecular ions plays also an non- negligible role. The main loss processes are electron impact excitation to 2p levels and resonance levels, then argon atom three-body collisional association reaction becomes the dominating loss channel when approaching the wall. Figure 8 shows radial profiles of production and loss processes of resonance state ($1s_4$) along the constrictor outlet. Electron impact 2p levels deexcitation and electron impact ground state and metastable state excitation are the dominating production process at first, then atom collision dissociation of excimers and electron impact ground state excitation and atom impact 2p levels deexcitation become the main production channel at the vicinity of wall. The dominating loss processes of $1s_4$ state are electron impact excitation to 2p levels at first, radiation of $1s_4$ state becomes main loss process and atom impact three-body collisional association reaction plays also a significant role near the constrictor wall.

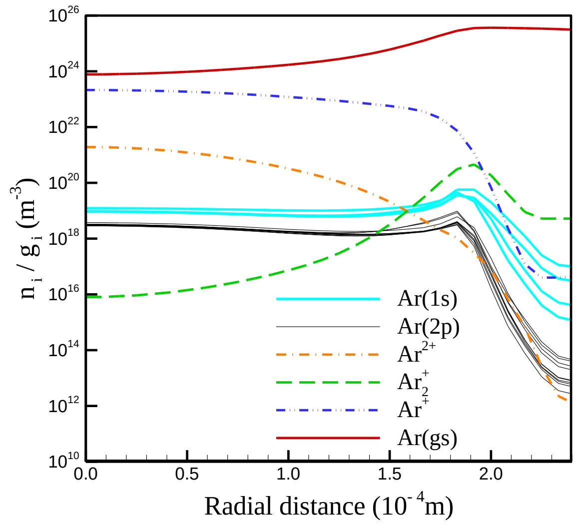

Figure 6. Radial profiles of plasma composition along the constrictor outlet.

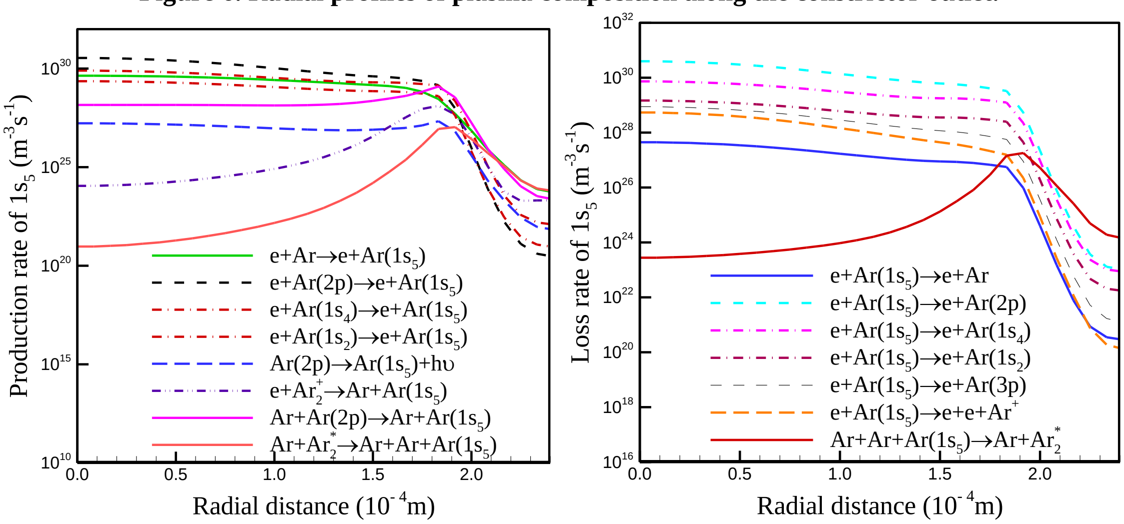

(a) (b)

Figure 7. Radial profiles of production (a) and loss (b) of $1s_5$ state along the constrictor outlet.

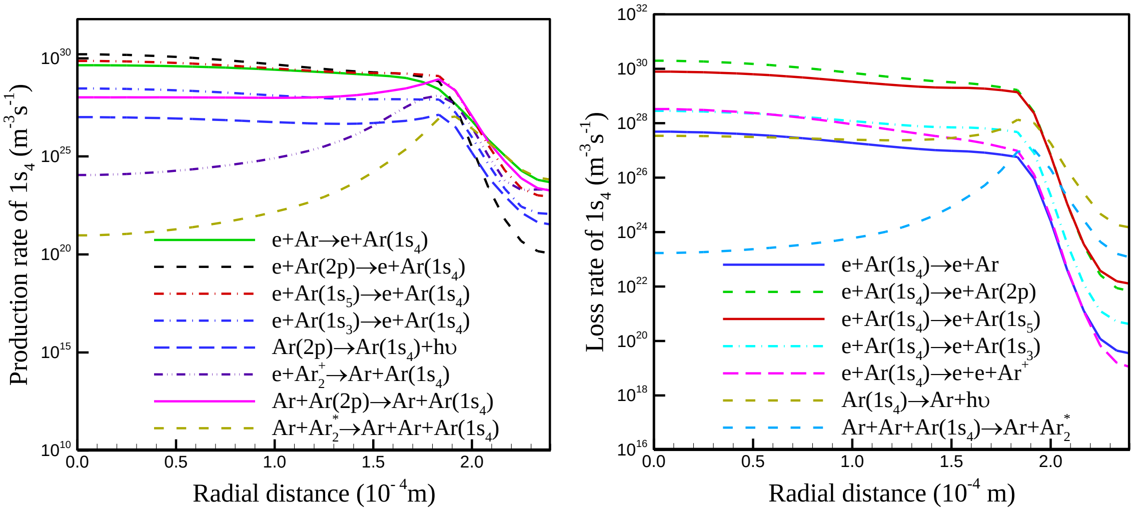

(a) (b)

Figure 8. Radial profiles of production (a) and loss (b) of 1s$_4$ state along the constrictor outlet.

H. Chemical kinetic processes inside expansion portion of the nozzle

Figure 9 shows axial profiles of plasma composition along arc attachment zone. In the first part of arc attachment, the number densities of molecular ions are higher than that of atomic ions. The number densities of excited states increase with electron temperature and the number densities of metastable state are the highest in this region. In the last part of arc attachment, the number densities of atomic ions become the highest. The number densities of molecular ions and excited states gradually decrease and the number densities of excimers can be neglected. Figure 10 shows axial profiles of ionization and recombination mechanisms along arc attachment zone. At the beginning of arc attachment, electron impact ground state atom ionization is the dominating ionization channel, whereas penning ionization of metastable state has also an important influence on total ionization mechanisms. Atom impact three-body recombination is the main recombination channel, and radiative recombination plays a minor role. In the last part of arc attachment, electron collision high lying excited states is the dominating ionization mechanism, whereas penning ionization of metastable state can be neglected. Atom collision three body recombination is still the main recombination mechanism, but electron impact three body recombination to highly excited states become more and more important. Figure 11 shows axial profiles of production and loss rate of molecular ions along arc attachment region. At the beginning of arc attachment, Ar_2^+ ions are mainly produced by *Ar* atomic to molecular ions conversion, and another important production process is the metastable-metastable associative ionization. Ar_2^+ ions are mainly destroyed by the electron impact dissociation to produce atomic ions, whereas dissociative recombination also has an influence on total loss mechanism. In the last part of arc attachment, atomic to molecular ions conversion become the most important production process. Other production processes can be neglected here. The loss of Ar_2^+ ions is mainly due to the direct electronic collision dissociation.

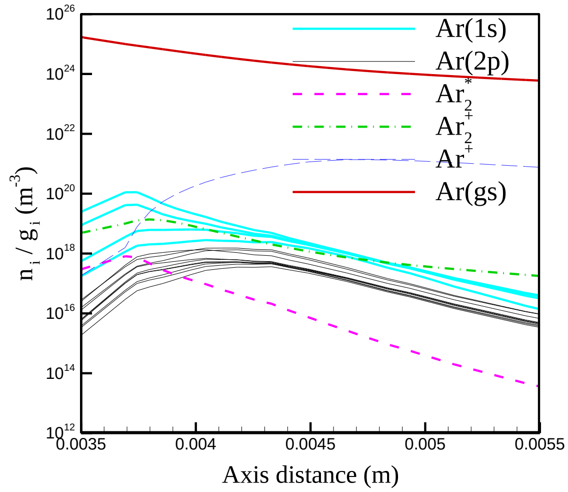

Figure 9. Axial profiles of plasma composition along arc attachment region.

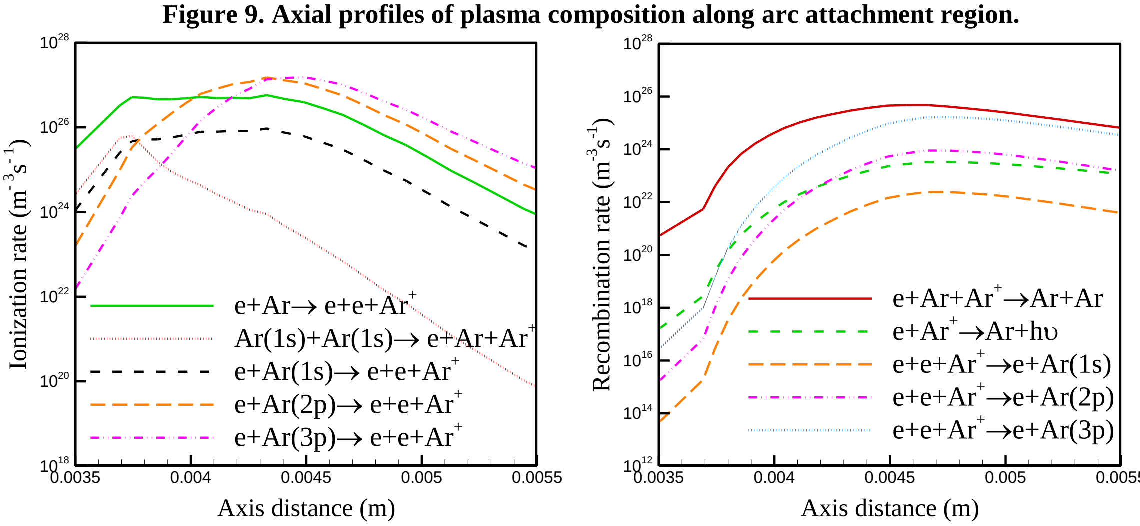

(a) (b)

Figure 10. Axial profiles of ionization (a) and recombination (b) mechanisms along arc attachment region.

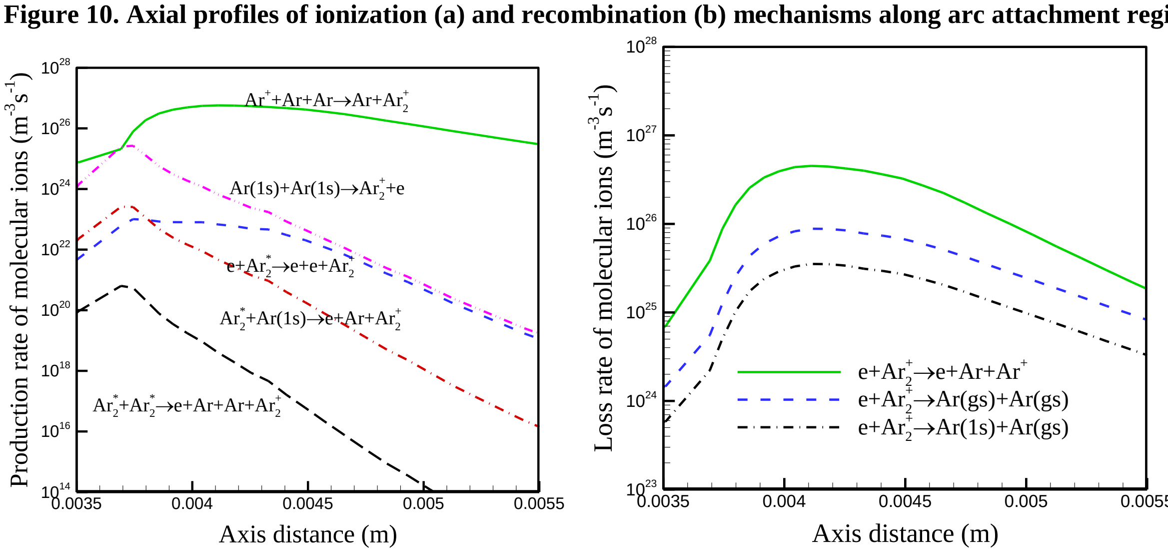

(a) (b)

Figure 11. Axial profiles of production (a) and loss (b) of molecular ions along arc attachment region.

Figure 12 shows axial profiles of plasma composition along the arcjet nozzle axis. The number densities of particles decrease with the increase of axial distance. The number densities of molecular ions and excimers are too low to be neglected. Figure 13 shows axial profiles of production and loss rate of $1s_5$ state along the arcjet nozzle axis. The main production processes of $1s_5$ state are due to electron impact 2p levels and resonance levels deexcitation. Electron collision three body recombination and atom impact 2p levels deexcitation play also a significant role at the first part. Spontaneous emission of 2p levels plays an important role nearby the wall. The main loss processes of $1s_5$ state are electron impact excitation to 2p levels and resonance levels. In the upstream of nozzle, electron impact excitation rate is higher than deexcitation rate, and electron impact three body recombination rate is lower than ionization rate. In the downstream of nozzle, electron impact deexcitation rate is higher than electron impact $1s_5$ excitation rate for 2p levels. Meantime electron impact three body recombination rate is higher than ionization rate.

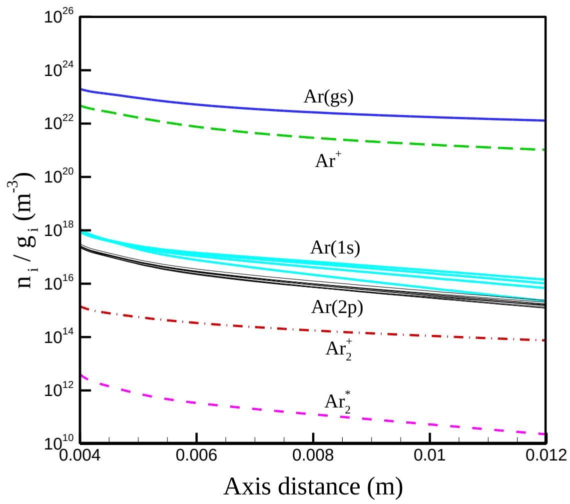

Figure 12. Axial profiles of plasma composition along the arcjet nozzle axis.

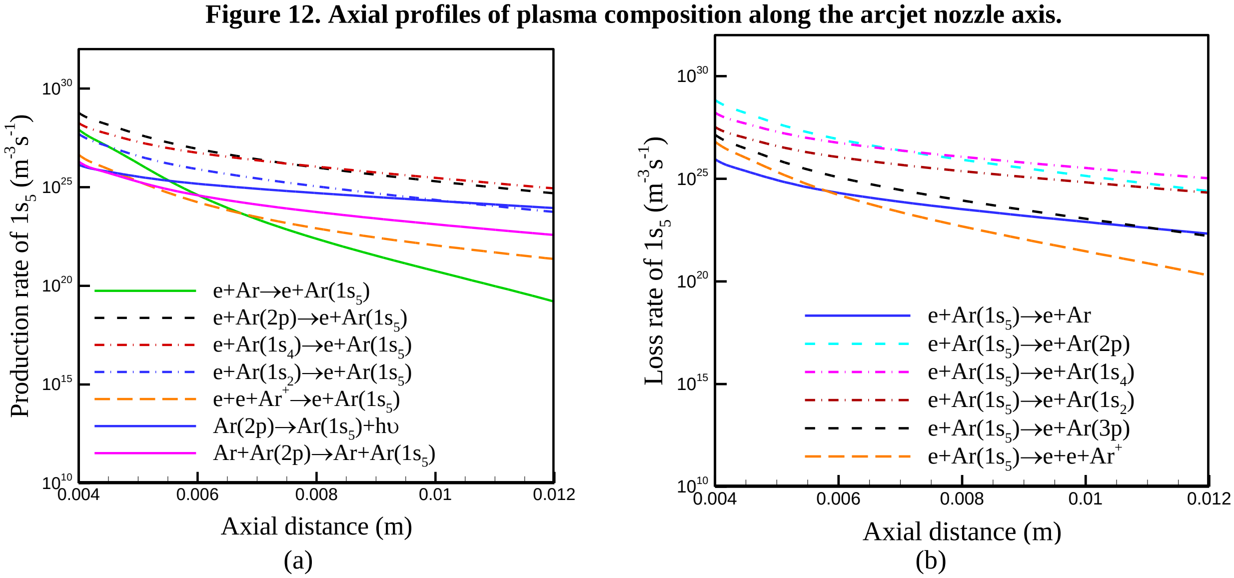

Figure 13. Axial profiles of production (a) and loss (b) rate of $1s_5$ state along the arcjet nozzle axis.

V. Conclusion

A simple argon collisional radiative model is applied to predict the population distribution and main kinetic processes in different parts of arcjet. In the constrictor axis the plasma is in an ionized state. Molecular ions and metastable state play an important role at the constrictor wall. Different kinetic processes exist in the arc attachment zone. Atom collision processes and penning ionization have a significant role in the beginning of arc attachment. In the upstream of expansion axis, the rate of ionization and excitation of metastable state is high due to the high electron temperature. The deexcitation and recombination processes of metastable state become more and more important with the increase of axis distance. A complete model including radiation trapping and transport phenomena is under study to better clarify the mechanism in arcjet. It is important that the excited level populations obtained allow for a direct and detailed optical diagnosis of the experiment in various parts inside the arcjet. A study of the experimentally evaluated populations in arcjet is needed to validate the results.

Acknowledgments

This work was supported by the National Natural Science Foundation of China. (Grant Nos. 11275021, 11072020, 50836007).

References

[1]Storm, P. V., Cappelli, M. A., "LIF Characterization of Arcjet Nozzle Flows," *32nd AIAA/ASME/SAE/ASEE, Joint Propulsion Conference and Exhibit*, AIAA-96-2987, Lake Buena Vista, FL, July, 1996.

[2]Cappelli, M. A., Storm, P. V., "Interior Plasma Diagnostics of Arcjet Thrusters," *Journal of Propulsion and Power*, Vol. 12, No. 6, 1996, pp. 1070-1076.

[3]Bates, D. R., Kingston, A. E., Mc Whirter, R. W., "Recombination between Electrons and Atomic Ions. I. Optically Thin Plasmas," *Proceedings of the Royal Society A*, Vol. 267, 1962, pp. 297-312.

[4]Colonna, G., Pietanza L. D., Capitelli M., "Coupled Solution of A Time-Dependent Collisional-Radiative Model and Boltzmann Equation for Atomic Hydrogen Plasmas: Possible Implications with LIBS Plasmas," *Spectrochimica Acta Part B*, Vol. 56, 1997, pp. 587-598.

[5]Bourdon, A., Vervisch, P., "Three-Body Recombination Rate of Atomic Nitrogen in Low-Pressure Plasma Flows," *Physical Review E*, Vol. 54, No. 2, 1996, pp. 1888-1898.

[6]Limbaugh, C. C., "Validity of the Quasisteady State and Collisional-Radiative Recombination for Helium Plasmas. I. Pure Afterglows," *Physical Review A*, Vol. 4, No. 6, December 1971, pp. 2368-2377.

[7]Kunc, J. A., Soon, W. H., "Collisional-Radiative Non-equilibrium in Partially Ionized Atomic Nitrogen," *Physical Review A*, Vol. 40, 1989, pp. 5822-5843.

[8]Wei, F. Z., Wang, H. X., Murphy, A. B., Sun, W. P., Liu, Y., "Numerical Modeling of the Nonequilibrium Expansion Process of Argon Plasma Arc through A Nozzle," *Journal of Physics D: Applied Physics* (submitted).

[9]Bultel, A., Annaloro, J., "Elaboration of Collisional-Radiative Models for Flows Related to Planetary Entries into the Earth and Mars Atmospheres," *Plasma Sources Science and Technology*, Vol. 22, 2013, 025008-1-025008-17.

[10]Chang, C. H., Ramshaw, J. D., "Numerical Simulation of Nonequilibrium Effects in An Argon Plasma Jet," *Physics of Plasmas*, Vol. 1, No. 11, November 1994, pp. 3698-3708.

[11]Vlcek, J., "A Collisional-Radiative Model Applicable to Argon Discharges over A Wide Range of Conditions. I: Formulation and Basic Data," *Journal of Physics D: Applied Physics*, Vol. 22, 1989, pp. 623-631.

[12]Bogaerts, A., Gijbels, R., "Collisional-Radiative Model for An Argon Glow Discharge," *Journal of Applied Physics*, Vol. 84, No. 1, July 1998, pp. 121-136.

[13]Zhu, X. M., Pu, Y. K., "A Simple Collisional-Radiative Model for Low-Temperature Argon Discharges with Pressure Ranging from 1 Pa to Atmospheric Pressure: Kinetics of Paschen 1s and 2p Levels," *Journal of Physics D: Applied Physics*, Vol. 43, 2010, pp. 015204-1-015204-17.

[14]Bultel, A., Ootegem, B. Van., Bourdon, A., Vervisch, P., "Influence of Ar_2^+ in An Argon Collisional-Radiative Model," *Physical Review E*, Vol. 65, 2002, pp. 046406-1-046406-16.

[15]Bond, J. W., "Structure of A Shock Front in Argon," *Physical Review*, Vol. 105, No. 6, March 1957, pp. 1683-1694.

[16]Wiese, W. L., Brault, J. W., Danzmann, K., Helbig, V., Kock, M., "Unified Set of Atomic Transition Probabilities for Neutral Argon," *Physical Review A*, Vol. 39, No. 5, March 1989, pp. 2461-2471.

[17]Haugsjaa, P., Amme, R., "Ionization and Metastable Excitation in Low Energy Collisions of Ground State Argon Atoms," *Journal of Chemical Physics*, Vol. 52, No. 9, May 1970, pp. 4874-4877.

[18]Dyatko, N. A., Ionikh, Y. Z., Kochetov, I. V., Marinov, D. L., Meshchanov, A. V., Napartovich, A. P., Petrov, F. B., Starostin, S. A., "Experimental and Theoretical Study of the Transition between Diffuse and Contracted Forms of the Glow Discharges in Argon," *Journal of Physics D: Applied Physics*, Vol. 41, 2008, pp. 055204-1-055204-14.

[19]Neeser, S., Kunz, T., Langhoff, H., "A Kinetic Model for the Formation of Ar_2 Excimers," *Journal of Physics D: Applied Physics*, Vol. 30, 1997, pp. 1489-1498.

[20]Lam, S. K., Zheng, C-E., Lo, D., Dem·yanov, A., Napartovich, A. P., "Kinetics of Ar_2^* in High-Pressure Pure Argon," *Journal of Physics D: Applied Physics*, Vol. 33, 2000, pp. 242-251.